WPT SAR Compliance Simulation Report for M-CM-AD-BK-2, M-CM-AA-BK-2, M-CM-AE-BK-2, M-CM-AF-BK-2, M-CP-AA-BK-2

M-CM-AD-BK-2, M-CM-AA-BK-2, M-CM-AE-BK-2, M-CM-AF-BK-2,

M-CP-AA-BK-2

FCC ID: 2AZ94MCMAA2

Date of Simulation: 2024-04-02

Note:

The test results in this test report relate only to the devices specified in this report. This report shall not be reproduced except in full without the written approval of CTTL.

Test Laboratory:

CTTL, Telecommunication Technology Labs, CAICT

No. 52, Huayuan North Road, Haidian District, Beijing, P. R. China 100191.

Tel:+86(0)10-62304633-2512, Fax:+86(0)10-62304633-2504

Email: cttl_terminals@caict.ac.cn, website: www.caict.ac.cn

TABLE OF CONTENT

1 Introduction

This report demonstrates RF exposure compliance using SAR simulation for WPT of M-CM-AD-BK-2, M-CM-AA-BK-2, M-CM-AE-BK-2, M-CM-AF-BK-2, M-CP-AA-BK-2 (FCC ID: 2AZ94MCMAA2)

The device is a transmitter wireless charging device. The DUT can provide wireless charging for a mobile phone. According to §2.1093 (certification for portable devices below 4 MHz), the device operating at 114.4–148.0 kHz & 354.2-369.4kHz should demonstrate RF exposure compliance to the 1.6 W/kg localized 1-g SAR limit. Therefore, to be conservative, we consider the device to be a portable device as a wireless charger. For portable devices, an accurate SAR value for the WPT transmitter is required. Since SAR test tools is not suitable for use below 100 MHz, we apply SAR numerical modeling to obtain SAR values.

The following sections describe the modeling, measured H-field, simulated H-field, and simulated SAR

2 Product Information

This is a device supporting wireless charging function. It can provide charging for other mobile phone through wireless charging. The Wireless power transfer application details are as below:

A. Wireless charging operating frequency

ANS: The wireless charging operating frequency range of the DUT is 114.4 kHz-148.0 kHz & 354.2 kHz-369.4 kHz.

B. Wireless charging maximum output power

ANS: When the DUT is used as the wireless charging Tx device, the maximum power of the wireless charging is 15W.

C. Wireless charging usage scenarios

ANS: The device is a transmitter wireless charging device. The DUT can provide wireless charging for a mobile phone. The DUT is used as a wireless charging transmitter device (Tx) in this usage scenario like Figure 1. The transfer system includes only single primary coil. The device only supports one to one pairing with the client device.

It is automatically turn on the wireless charging TX function when a client device placed directly in contact with the front side charging area of TX device.

Figure 1. DUT Used as a wireless charging transmitter device

D. Wireless charging standard and operating diagram

ANS: The operating diagram of the wireless charging DUT is as below picture:

The adapter supplies power to the transmitter side and converts AC to DC by protocol. The transmitter converts DC to AC by using the LC charge/discharge circuit, which provides the transmitter coil to generate a magnetic field. The receiving coil couples AC power within the magnetic field, and provides it to the RX chip. The RX uses the rectifier output DC to charge the mobile phone.
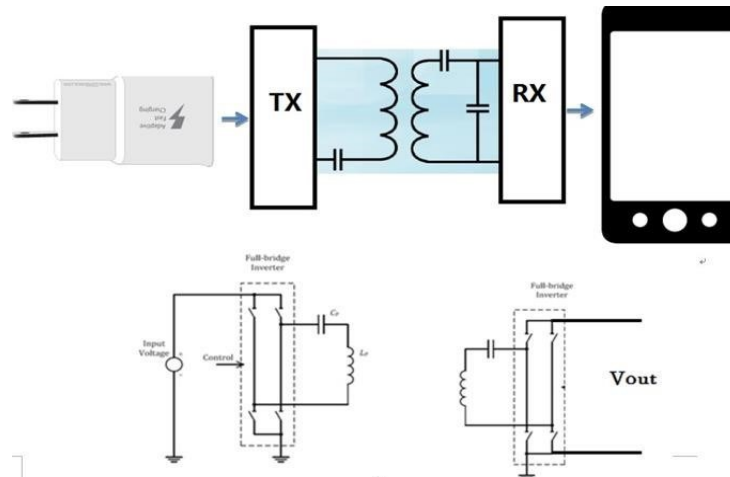

Figure 2. The wireless charging operating diagram

E.　The number of turns for the primary coils, the amperes into the coil, and primary and secondary coil alignment and separation requirements.

ANS: The device has only one coil and the number of turns for the primary coil is 11 turns. The coil in DUT has 1.1A current while the DUT is operating in maximum output power.

F.　Details on how charging is initiated and managed.

ANS: When the charging function (Tx mode) is enabled：

1.　The wireless charging IC is powered on, and identifying the adapter type.

2.　Then the PING frequency, the PING duration and the PING interval time are set.

3.　The OCP (over current protection) and OVP (over voltage protection) parameters are set, the PING signal is sent, and the transmission is continued.

4.　Once the PING is successful, the transmitting adjusts the transmission frequency according to the CEP (Control Error Packet) packet sent by the RX to establish a wireless power transmission.

5.　Once RX is removed, TX re-enters the PING phase.

G.   Detail information of the RF exposure analysis the coil design to simulate the actual coil.

ANS: The coil module is composed of an FPC coil and a ferrite shielding material, and the magnetic shielding material blocks the magnetic field in the direction behind the coil.
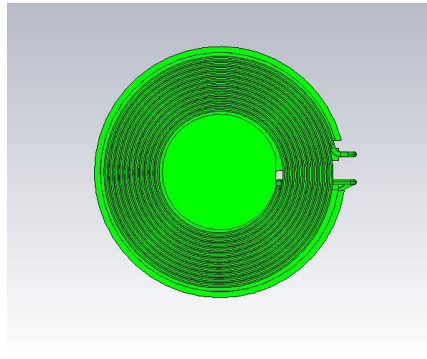

Figure 3. Coil Schematic

H.   Description on the message exchanges between the transmitter and the receiver

ANS: Tx and Rx communicate using a single channel, and all Rx-Tx and Tx-Rx communication physical channels are wireless signals transmitted by Tx. Rx-Tx is AM (Amplitude Modulation) communication, and Tx-Rx is FM (Frequency Modulation) communication. During the handshake, Rx sends a Signal Strength Packet, ID Packet, and Config Packet to the Tx. After the handshake is successful, Rx sends RPP (Received Power Packet) and CEP (Control Error Packet) to adjust the power.

3 Simulation Tool and Model

3.1 Simulation Tool

For the calculation of the magnetic field value and SAR simulation method of the DUT with the function of wireless charging, this article uses the electromagnetic module in CST STUDIO SUITE 2019. CST STUDIO SUITE 2019 is one of several commercial tools for 3D electromagnetic simulation of wireless charging. The low frequency domain solver in CST STUDIO SUITE 2019 is based on finite element method (FEM) solution.

3.2 Mesh and Convergence Criteria

To use FEM to calculate the magnetic field value and SAR value of wireless charging, it is necessary to divide the charging device, human tissue, and surrounding environment into multiple small units. The physical quantities on the nodes and edges of each small unit can be used as the calculated magnetic field value and the process of dividing the unknown SAR value into small cells is called meshing. In order to calculate the objective of the solution, the CST STUDIO SUITE 2019 adaptive meshing technique was used. CST STUDIO SUITE 2019 generates an initial mesh based on the minimum value of the wavelength of the electromagnetic field and the size of the target body, calculates the energy error during each iteration, and performs adaptive refinement and refinement for the regions with large errors. The determination of the number of calculation iterations in CST STUDIO SUITE 2019 and the completion of the final iterative calculation process are called the convergence process. The convergence criterion tolerance is used to judge whether the convergence process is over. During the calculation process, the iterative adaptive grid process is performed until the convergence criterion tolerance is met. In CST STUDIO SUITE 2019, the accuracy of the convergence results depends on the tolerance. Figure 4 is an example of computing an object adaptive mesh.
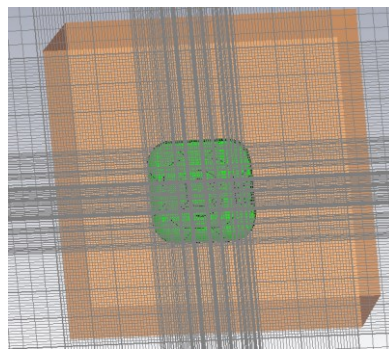

Figure 4. an example of computing an object adaptive mesh.

3.3 Power Loss Density Calculation

By solving the three-dimensional wireless charging reverse charging simulation model, the numerical values of the electric field and magnetic field physical quantities at each position in the space can be obtained. In order to calculate the power density, two physical quantities need to be extracted: the electric field ($\vec{E}$) and the magnetic field ($\vec{H}$). The actual power density dissipated as the complex conjugate product of the electric field E and the magnetic field H yields the real part of the vector ($\vec{S}$) as follows:

$$\vec{S} = \frac{1}{2} Re(\vec{E} \times \vec{H})$$

$\vec{S}$ is the power density at the node is calculated for each mesh, which can be obtained directly from CST STUDIO SUITE.

From the point power density $\vec{S}$, the calculation formula of the average power density of the space volume V is as follows:

$$P = \frac{1}{V} \iiint \vec{S} \cdot dV$$

Here, the spatial average power density P is the total power density value of the x, y, and z components of the point power density, and the estimated volume is 1 cm3.

3.4 3D Model

Figure 5 shows the 3D simulation model of wireless charging device. The simulation model includes most of the finishing structure of the device: PCB, plastic frame, metal structure, wireless charging coil and magnetic conductive material, etc.
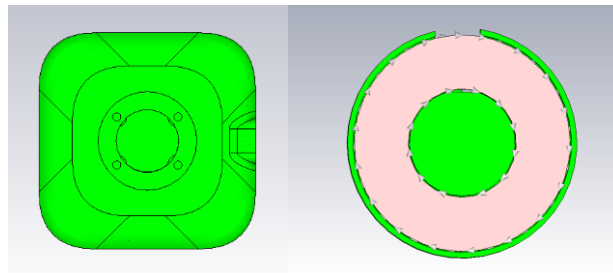

Figure 5. The 3D simulation model of wireless charging device and wireless charging coil

4 SAR Simulation Step

4.1 SAR Simulations Methodology

The following Figure are taken to show the validity of the model used for SAR simulations：
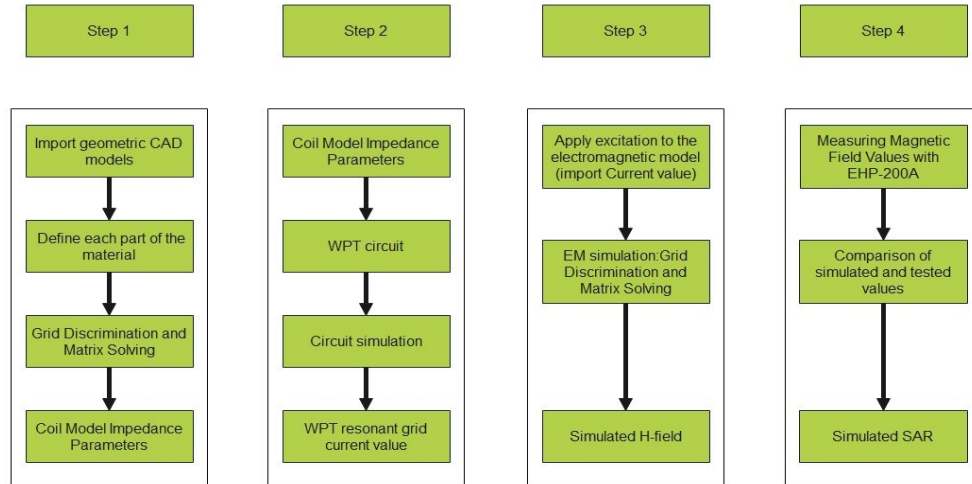

Figure 6. The steps of SAR simulation

First, the CAD model of the wireless charging device is imported into the software for material definition and mesh division to calculate the impedance of the coil. Then import the coil impedance into the WPT circuit to calculate the current value of the WPT circuit. And then, the electromagnetic model is excited by the current, and the simulated value of the field strength can be obtained. The accuracy of the wild goose array simulation is compared by the simulation and the actual measurement, and finally the SAR value is simulated.

4.1.1 Boundary Conditions

FEM-based electromagnetic simulation tools need to impose boundary conditions on the simulation model, and the boundary conditions imposed are the first type of boundary conditions (Dirichlet boundary conditions). CST STUDIO SUITE 2019 supports the direct application of Dirichlet boundary conditions.

4.1.2 Source Excitation Condition

The excitation conditions for wireless charging calculation are obtained by the circuit as shown in Figure 6. Calculated current excitation results of the circuit can be applied directly at the coil port. After completing a 3D full-wave electromagnetic simulation of the modeled structure, the current to the coil can be loaded using the CST STUDIO SUITE 2019 "low frequency source" function. Since CST STUDIO SUITE 2019 uses a FEM solver based on the frequency domain analysis method, the input source of the coil excitation is calculated using a sinusoidal waveform for the operating frequency.

4.1.3 Simulation Completion Conditions

The simulation completion condition in CST STUDIO SUITE 2019 is defined as a tolerance smaller than the desired value. The simulation result for this report is to set the tolerance to 1e-6.

4.2 H-field Strength Measurement and Simulations

We use the Narda EHP-200A to measure the actual H-field strength of the DUT. EHP-200A E-H fields analyzer has been designed for accurate measurements of both electric (0.02 to 1000 V/m) and magnetic (3 mA/m to 300 A/m) fields in the frequency range 9 kHz to 30 MHz. Both the field sensors and the electronic measuring circuitry are accommodated in a robust housing. Measurements are given total value (peak and average), with exceptional flatness and linearity. The probe specifications of H-field mode are giving below:

Test Mode	Magnetic Field Mode A
Frequency range	9 kHz-3 MHz
Measurement range @10 kHz RBW	30 mA/m – 300 A/m
Dynamic range	> 80 dB
Resolution	1 mA/m
Sensitive @10 kHz RBW	30 mA/m
Flatness	0.8 dB
Span	0 to Full Span

Table 1 The information of EHP-200A for H-field measurement

For the EHP-200A the sensitive element is located approximately 8 mm bellow the external surface like Figure 7, therefore, when comparing the simulated values, the simulated field strength should be obtained at 8 mm from the surface of the DUT. Per TCB Workshop April 2022, If the center of the probe sensing element is more than 5 mm from the probe outer edge, the field strengths need to be estimated for the positions that are not reachable (from the surface, in 2 cm increments)
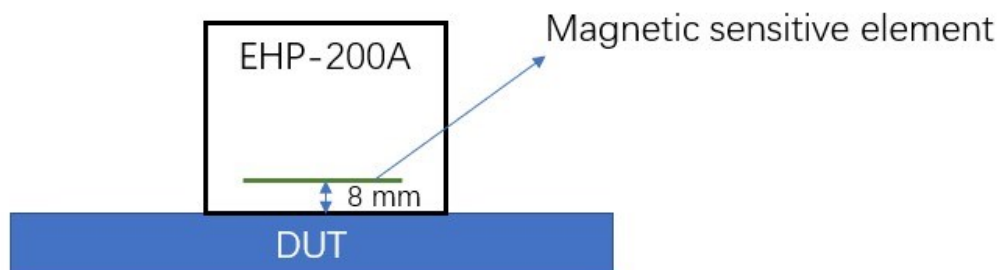

Figure 7. The located of sensitive element

When the charging device is close to the DUT device, the is activated. Start testing the DUT when operating at maximum transmit power. The front, back, left, right, top and bottom sides of the test are defined as shown in Figure 8.
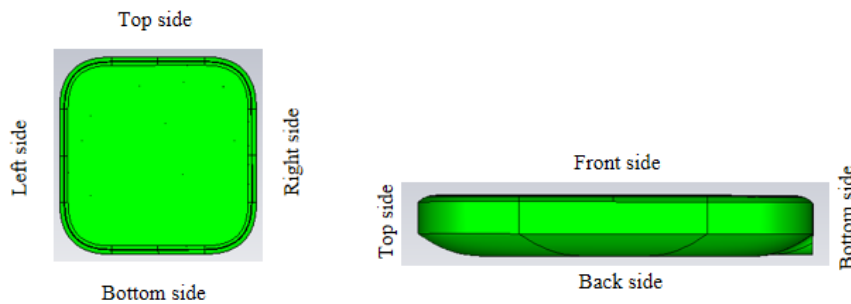

Figure 8. DUT test diagram

To accurately measure the value of the magnetic field strength, we set the measurement step to 2 cm, and the test surface is the Front, Back, Right,Left,Top and Bottom sides that conform to the Portable device. Each point is repeat measured three times.

The H-field simulations are conducted using commercially available software CST STUDIO SUITE. To validate the simulation model, H-field measurements are made on the DUT and compared to the simulated results (as shown in Figure 9). The validated model is then used for SAR simulations.

For wireless charging, the maximum transmit power of Tx is 15W. Although the conditions for this scenario are very harsh, considering the worst case, it needs to be simulated. The measured result and simulation result are shown below. The bottom side of the DUT needs to be connected to the power supply line, so it cannot be measured. A 35mm support frame is provided on the back side of the DUT. It can be seen that the biggest gap between simulation and test is only 19%, which is far below the requirement of 30% (per April 27, 2022, TCB Workshop). In this case the H-field strength values of the four sides are in good agreement with the simulated values. So, this mode can be used to calculate SAR values.

Test/simulation Side	Test Channel/Freq (kHz)	Test Tx Power (W)	Horizontal offset (mm)	Test Result (A/m)	Simulation Result (A/m)	Gap (%)
Front Side	361.4	15	0	5.83	6.14	5.3%
Back Side	361.4	15	35	0.21	0.25	19%
Left Side	361.4	15	0	1.22	1.24	1.6%
Right Side	361.4	15	0	1.06	1.23	16%
Top Side	361.4	15	0	1.61	1.90	18%
Bottom Side	361.4	15	0	-	-	-

Table 2. The Test and simulation result of H-field at 15W

Per TCB Workshop April 2022, If the center of the probe sensing element is more than 5 mm from the probe outer edge, the field strengths need to be estimated for the positions that are not reachable (from the surface, in 2 cm increments). Therefore, we did a simulation test comparison from 8 mm (the distance between the magnetic induction unit from the DUT surface) to 12 cm on the front side surface of 15 W. The results are shown in the following figure. The figure shows good correlation between the measurements and simulations.
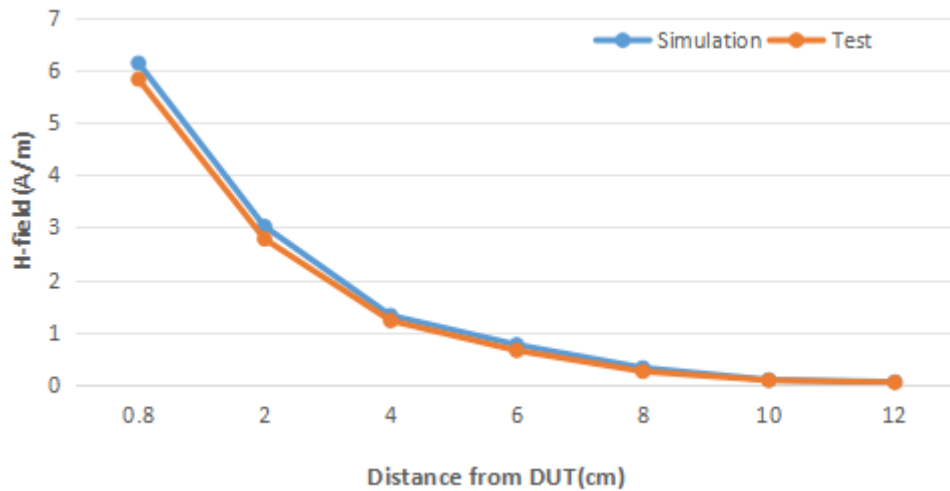

Figure 9. Comparison of test and simulation at different distances at 15 W

4.3 SAR simulation

The SAR simulations are conducted using commercially available software CST STUDIO SUITE by same model. For this simulation, a phantom is added in contact with the DUT.

The following steps are used for accurate SAR simulation:

1) Homogenous tissue material is used as liquid for desired frequency.

2) Power loss in phantom is calculated.

3) SAR can be calculated by the Equation:

$$SAR = \frac{P}{\rho}$$

where P is the Power loss density, and ρ is the tissue density.

4) SAR is averaged over 1 g at 0 mm (FCC).

The portable scene during charging appears when holding a mobile phone to make a call or placing it on the body to use the mobile phone. Therefore, it is necessary to determine the electrical properties of phantom. As mentioned earlier, the frequency of wireless charging is 361.4 kHz, so the electrical characteristics of the body and hand at this frequency are summarized as follows:

Tissue	Thickness (mm)	Permittivity	Conductivity(S/m)
Skin	3	1114.62	0.17
Muscle	9	7428.41	0.355
Bone	20	433.88	0.082
Worst case	/	7428.41	0.355

Table 3. The electrical characteristics for body layers

For hand phantom, compared with body layers, the thickness of each layer is different, but the electrical characteristics are the same at the same frequency, so the same worst case can be used. For all exposure cases, conductivity and permittivity used for the phantoms are fixed as the worst case (0.355 S/m and 7428.41), and the phantom thickness is 100 mm. And the SAR results are peak spatial 1-gram average SAR.

The worst use case is at 15 W, we made SAR simulations for the 15W case without horizontal offset. The results are shown below:

Simulation Side	Tx Power (W)	Peak Spatial Average SAR over 1-g (W/kg)
Front Side	15	5.65E-03
Back Side	15	6.06E-04
Left Side	15	8.65E-05
Right Side	15	8.65E-05
Top Side	15	9.84E-05
Bottom Side	15	-

Table 4. The Peak spatial average SAR result calculated by simulation

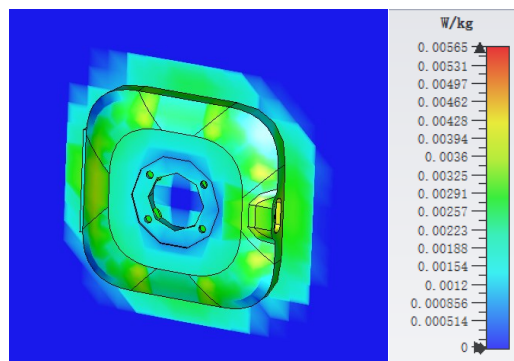SAR plot is show below (Front side without offset).

Figure 10. SAR distribution for back side without offset.

4.4 Calculation

The accuracy of the SAR simulations is demonstrated by correlating H-field measurements to simulations in Figure 9, Figure 10, Table 2 and Table 4. For the case where the phones have no Horizontal offset, the highest peak spatial 1-g average SAR is 5.65E-03 W/kg, well below FCC SAR limit 1.6 W/kg.

Annex A: specific information for SAR computational modelling

1) Computation Resources

The models were simulated on a 20 core CPU server with an available RAM of 64 GB. Each model variation took around 14 hours to complete. Based on the simulation profile, the minimum resources needed to finish these simulations will be approximately 8 core CPU with 16 GB of RAM. Using the minimum requirements simulation will likely take more time than 14 hours.

2) Algorithm implementing and validation

This section is divided into two parts. The code performance validation provides methods to determine that the finite-element algorithm in CST has been implemented correctly and works accurately within the constraints due to the finite numerical accuracy. It further determines the quality of absorbing boundary conditions and certain parts of the post processing algorithms that are part of CST. The second part has few canonical benchmarks. All benchmarks can be compared to analytical solutions of the physical problem or its numerical representation. The methods characterize the implementation of the finite-element algorithm used by CST in a very general way. They are defined such that it is not possible to tune the implementation for a particular benchmark or application without improving the overall quality of the code.

2.1) Code performance validation

2.1.1) Propagation homogeneous medium

A straight rectangular waveguide with ports on both ends is well suited as a first test of an implementation of the Finite-Element Method used by CST. The waveguide has a width of 20 mm, a height of 10 mm and a length of 300 mm. The waveguide is filled homogeneously with a material which, in three separate simulations, shall assume the following properties:

      i. $\varepsilon_r = 1$, $\sigma = 0$ S/m;

      ii. $\varepsilon_r = 2$, $\sigma = 0$ S/m;

      iii. $Re(\varepsilon_r) = 2$, $\sigma = 0.2$ S/m.

To verify that the mesh used by CST is independent of orientation, the waveguide has been rotated so that it is not parallel with any principal coordinate plane (XY, XZ, YZ). The waveguide is driven in the TE10 mode at 10 GHz. Reported are the magnitudes of S21 and S11, as well as the values of the real and imaginary parts of the propagation constant γ. The table 5, below provides the reference values, acceptable result criteria, as well as the simulated results.

Table 5:Criteria for the waveguide evaluation

$Re(\varepsilon_r)$	1	2	2
σ	0	0	0.2
|S21| reference value	1	1	8.7×10^{-5}
Criterion for |S21|	≥ 0.9999	≥ 0.9999	$\pm 5 \times 10^{-6}$
|S21| simulated results	1	1	8.7×10^{-5}
|S11| reference value	0	0	0
Criterion for |S11|	≤ 0.003	≤ 0.003	≤ 0.003
|S11| simulated results	0	0	0
$Re(\gamma)$ reference value	0	0	$31.17 m^{-1}$
Criterion for $Re(\gamma)$	$\pm 0.1 m^{-1}$	$\pm 0.1 m^{-1}$	$\pm 2\%$
$Re(\gamma)$ simulated results	0	0	31.17
$Im(\gamma)$ reference value	$138.75 m^{-1}$	$251.35 m^{-1}$	$253.28 m^{-1}$
Criterion for $Im(\gamma)$	$\pm 2\%$	$\pm 2\%$	$\pm 2\%$

[Im(γ) simulated results	138.75	251.35	253.28

As is seen in the above table, CST easily meets the criteria for properly and accurately calculating the waveguide problem.

2.1.2) Planar dielectric boundary

In order to test the reflection of a plane wave by a dielectric boundary, a rectangular waveguide can again be used. It is well known that the TE10 mode can be thought of as a superposition of two plane waves. Each wave's direction of propagation makes an angle θ with the axis of the wave guide, given by

$$\cos^2\theta = 1 - (c/2af)^2 \tag{1}$$

where c is the speed of light, a is the width of the wave guide and f is the frequency. Assuming the axis of the waveguide is the Z axis and assuming the waveguide is filled with vacuum for Z>0 and filled with dielectric 1 with complex relative permittivity ε_r for Z<0, Fresnel reflection coefficients for the TE and the TM cases, defined as ratios of electric field strengths, are given by

$$R^{TE} = (k_{0,z} - k_{1,z}) / (k_{0,z} + k_{1,z}) \tag{2}$$

$$R^{TM} = (\varepsilon_r k_{0,z} - k_{1,z}) / (\varepsilon_r k_{0,z} + k_{1,z}) \tag{3}$$

where k0,z and k1,z denote the z component of the propagation vector of the plane wave in vacuum and in the dielectric, respectively. They can be evaluated through

$$k_{0,z} = k_0 \cos\theta \tag{4}$$

$$k_{1,z} = k_0 \sqrt{(\varepsilon_r - \sin^2\theta)} \tag{5}$$

Finally, ε_r is complex and is given by

$$\varepsilon_r = Re(\varepsilon_r) - j\sigma/(2\pi f \varepsilon_0) \tag{6}$$

where Re(ε_r) denotes the real part of the relative permittivity and σ is the conductivity of the medium.

For this test, a 20 mm × 10 mm waveguide with a length of 60 mm, as shown in Figure 11, was created. The top half was filled with vacuum and the bottom half with dielectric.
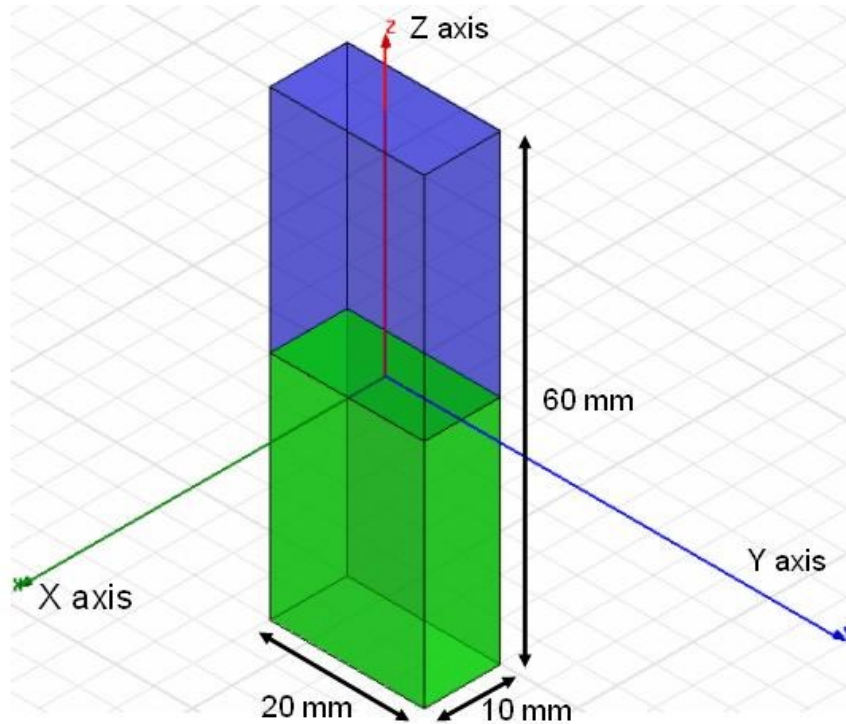

Figure 11: Waveguide filled half with vacuum and half with dielectric

In one copy of the model, all side walls were lossless metal, such that the dominant mode is the TE10 mode with propagation constant 138.75 m-1 at 10 GHz and represents the TE case in the reflection

analysis. In the other copy of the model, the side walls that are parallel to the YZ plane were perfect magnetic conductors while the other walls were perfect electric conductors, such that the *second* mode (after a TEM mode which won't be used in this test) has propagation constant 138.75 m-1 at 10 GHz and represents the TM case in the reflection analysis.

Before simulation, the waveguides were rotated over an arbitrary angle such that no face is parallel with any coordinate plane. The waveguides were driven at 10 GHz in the proper mode. In doing so, it is good practice to calculate all propagating modes, but the coupling between modes is expected to be negligible. Simulations were run for the cases of lossless and lossy dielectric as shown in Table 6. For the CST to pass the test, according to IEC 62704-1[1], the results need to be within 2% of the analytical values given in Table 2.

Table 6: Reflection at a dielectric interface

Re(εr)	σ (S/m)	RTE	RTE- Simulated	RTM	RTM - Simulated
4	0	0.4739	0.4739	0.1763	0.1763
4	0.2	0.4755	0.4755	0.1779	0.1779
4	1	0.5105	0.5105	0.2121	0.2121

As can be seen in table 2, CST produces results that are identical to the analytical results.

2.2) Canonical Benchmarks

The results for few low frequency benchmarks are summarized below. These benchmarks were used to validate the accuracy of the tool at low frequencies:

2.2.1) Dipole Antenna:

The following parameter were used in the dipole antenna to resonate at 400KHz.

Dipole length: 375 meters
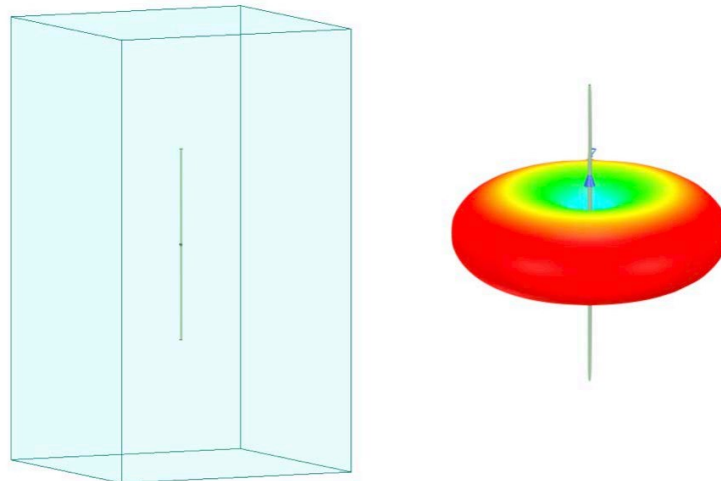
Feed gap: 2.5 meters

Dipole Diameter: 5 meters

Figure 12: Dipole Antenna Model

The document IEC 62704-4, 2020[2] was referenced to compare the tables. Two computation methods were demonstrated as shown below to show the validity of the model.

Table 3: Simulated Dipole parameters

FEM Solver

Quantity	Simulation results	Tolerance	Satisfied?
Re(Z) at 400 KHz	94.09		
Im(Z) at 400 KHz	55.62		
Re(Z) at 320 KHz	39.26	$25\Omega < Re(Z) < 50\Omega$	Yes
Im(Z) at 320 KHz	-90.52	$-50\Omega < Im(Z) < -100\Omega$	Yes
Re(Z) at 360 KHz	59.58	$50\Omega < Re(Z) < 75\Omega$	Yes
Im(Z) at 360 KHz	-18.30	$-25\Omega < Im(Z) < 0\Omega$	Yes
Frequency for Im(Z) =0	370	$360MHz < f < 380MHz$	Yes
Maximum power budget error	0.3	$< 5\%$	Yes

MoM Solver

Quantity	Simulation results	Tolerance	Satisfied?
Re(Z) at 400 KHz	98.45		
Im(Z) at 400 KHz	53.57		
Re(Z) at 320 KHz	43.31	$25\Omega < Re(Z) < 50\Omega$	Yes
Im(Z) at 320 KHz	-90.55	$-50\Omega < Im(Z) < -100\Omega$	Yes
Re(Z) at 360 KHz	65.03	$50\Omega < Re(Z) < 75\Omega$	Yes
Im(Z) at 360 KHz	-18.59	$-25\Omega < Im(Z) < 0\Omega$	Yes
Frequency for Im(Z) =0	370	$360MHz < f < 380MHz$	Yes
Maximum power budget error	0.02	$< 5\%$	Yes

2.2.2) Toroid Inductor:

The parameters of the toroid were chosen to be

N = 20

A = 6.35e-4 m^2

R = 0.0263 m

ur = 64

The formula below gave an inductance of 139uH. The model created in CST gave an inductance of 139.9uH.
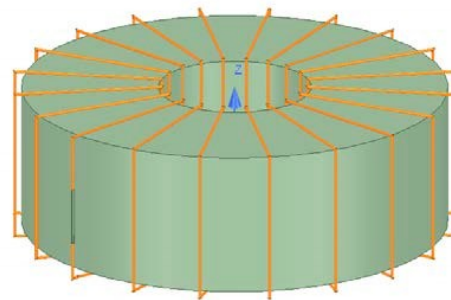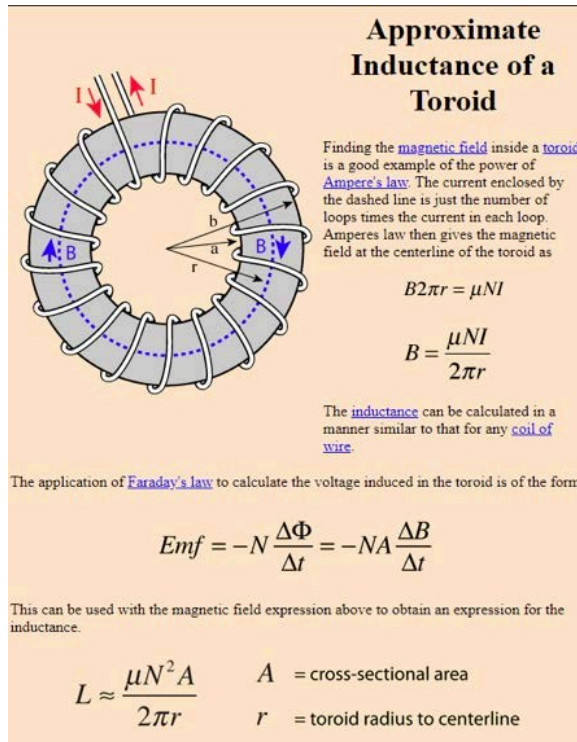
Figure 13: Toroid Model

2.2.3) Circular coil parallel to a flat, homogeneous phantom:

The following benchmark is implemented using Equations 1-4 of the referenced Chen et al. (2014) paper and also matches Figure 14 therein scaled to 10 coil turns.

Below is the coil and phantom parameters:

Coil Diameter: 50 mm

Number of Turns: 10

RMS Current: 0.707 A (Peak current = 1 A)

Frequency: 100 kHz

Coil-to-Body Distance: 5 mm

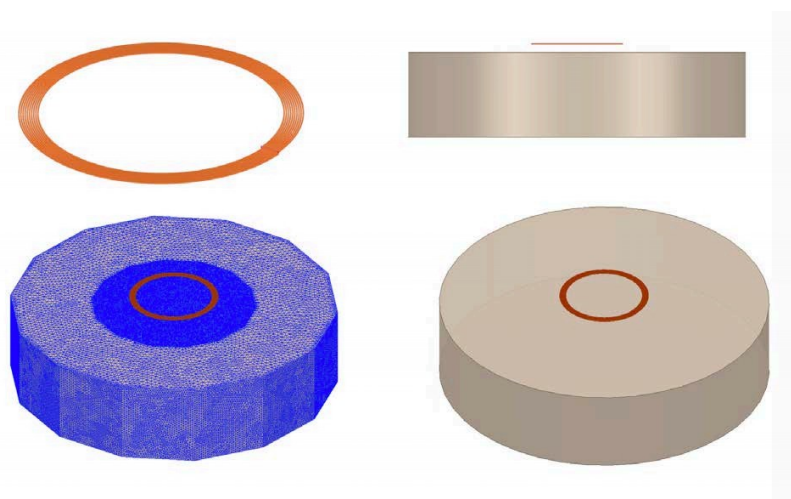Tissue Conductivity: 0.05 S/m

Tissue Permittivity: 1120

Figure 14: Current loop in front of a cuboid

The simulated spatial peak RMS electric field in tissue is 1.51 V/m compared to the analytical 1.47 V/m.
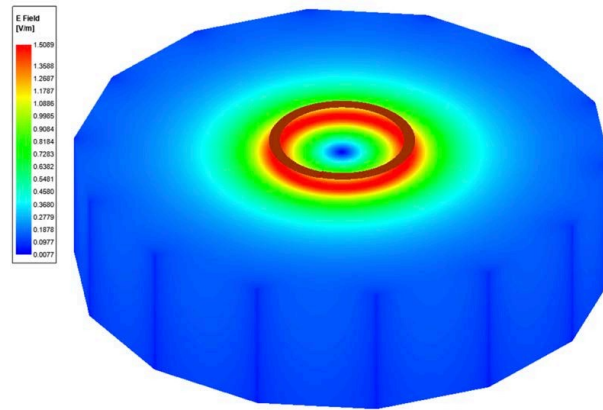
Figure 15: Current Density plot

3) Computational peak SAR from peak components & One-gram averaged SAR procedure

The calculation method for SAR follows IEEE P1528.4. Once the solver calculated the SParameter results, different coils can be driven and the result from the S-Parameter calculation is automatically scaled to the driving current of the coils. This result combination provides the correctly scaled power loss density in the phantom. The SAR calculation computes the local SAR first using electric field and conducting current:

$$SAR = \vec{E} \bullet \vec{J}_{conj} / (2\rho) \tag{7}$$

Afterwards the local SAR is averaged over a specific mass, usually 1g or 10g. As described in [IEEE P1528.4] the mass averaging is done by mapping the results to a structured hexahedral grid and afterwards the averaging scheme for FDTD per [IEEE P1528.4] is applied. The SAR calculation on the hexahedral grid is compliant with IEC 62704-1.
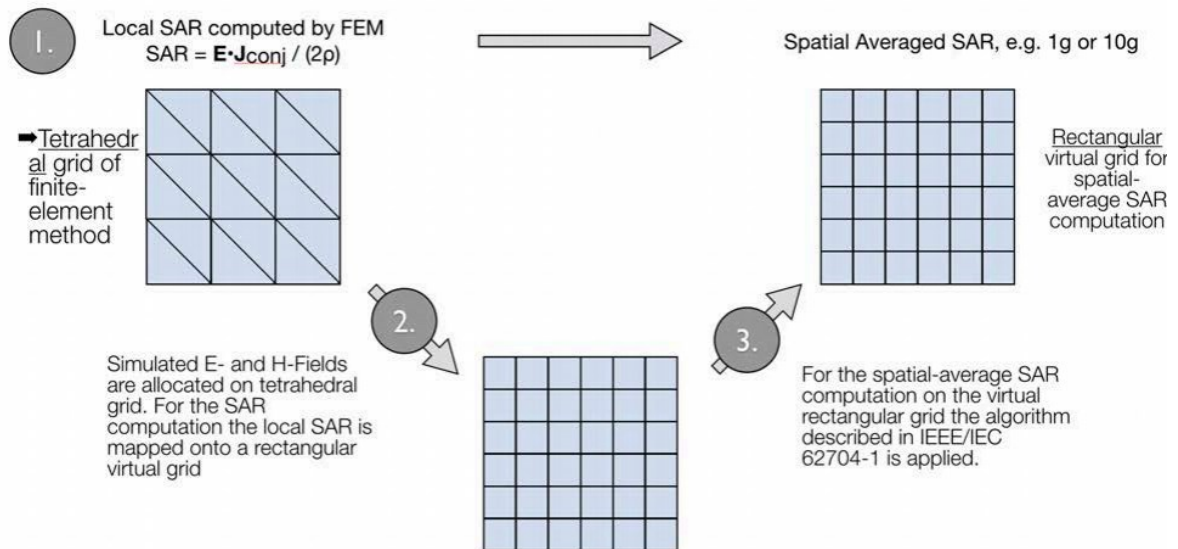

Figure 16: IEEE P1528.4 for SAR computation

4) Total Computational Uncertainty

Below is a table summarizing the budget of the uncertainty contributions of the numerical algorithm and of the rendering of the simulation setup. The table was filled using the IEC 62704-4, 2020.

For the simulations, the extreme case where the phantom is placed directly in front of the device is considered.

Table 7. Budget of uncertainty contributions of the numerical algorithm (filled based on IEC 62704-4 2020).

a	b	d	e	g
Uncertainty component	Subclause	Probability distribution	Divisor f(d, h)	Uncertainty %
Mesh resolution	7.2.2	N	1	1.5
ABC	7.2.3	N	1	0.2
Power budget	7.2.4	N	1	3.8
Convergence	7.2.5	R	1,73	1.63
Phantom dielectrics	7.2.6	R	1,73	0
Combined standard uncertainty (k= 1)				7.13

Below is a table summarizing the budget of the uncertainty of the developed model of the EUT so far. The table was filled using the IEC 62704-4, 2020.

Table 8. Uncertainty of DUT Model

a	b	d	e	g
Uncertainty component	Subclause	Probability distribution	Divisor f(d, h)	Uncertainty %
Uncertainty of the DUT model (based on near field distribution)	7.2.2	N	1	2.3
Uncertainty of the measurement equipment and procedure	7.2.3	N	1	4
Combined standard uncertainty (k= 1)				6.3

Table 9. Expanded Standard Uncertainty

a	b	d	e	g
Uncertainty component	Subclause	Probability distribution	Divisor f(d, h)	Uncertainty %
Uncertainty of the test setup with respect to simulation parameters	7.2	N	1	7.64
Uncertainty of the developed numerical model of the test setup	7.3	N	1	3.72
Combined standard uncertainty (k= 1)				11.36
Expanded standard uncertainty (k= 2)				22.72

References:

1) "IEC/IEEE International Standard -- Determining the peak spatial-average specific absorption rate (SAR) in the human body from wireless communications devices, 30 MHz to 6 GHz - Part 1: General requirements for using the finite-difference time-domain (FDTD) method for SAR calculations," in IEC/IEEE 62704-1:2017 , vol., no., pp.1-86, 27 Oct. 2017, doi: 10.1109/IEEESTD.2017.8088404.

2) "IEC/IEEE International Standard - Determining the peak spatial-average specific absorption rate (SAR) in the human body from wireless communication devices, 30 MHz to 6 GHz – Part 4: General requirements for using the finite element method for SAR calculations," in IEC/IEEE 62704-4:2020 , vol., no., pp.1-104, 19 Oct. 2020, doi: 10.1109/IEEESTD.2020.9237217.